Eur. Phys. J. Plus (2017) **132**: 265
DOI 10.1140/epjp/i2017-11519-4

THE EUROPEAN PHYSICAL JOURNAL PLUS

Regular Article

Melting heat transfer in the MHD flow of a third-grade fluid over a variable-thickness surface

Tasawar Hayat[1,2], Asmara Kiran[1], Maria Imtiaz[3,a], Ahmed Alsaedi[2], and M. Ayub[1]

[1] Department of Mathematics, Quaid-I-Azam University 45320, Islamabad 44000, Pakistan
[2] Nonlinear Analysis and Applied Mathematics (NAAM) Research Group, Department of Mathematics, Faculty of Science, King Abdulaziz University, Jeddah 21589, Saudi Arabia
[3] Department of Mathematics, University of Wah, Wah Cantt 47040, Pakistan

Received: 15 February 2017 / Revised: 24 April 2017
Published online: 14 June 2017 –

Abstract. The present study addresses the magnetohydrodynamic (MHD) flow of a third-grade fluid over a nonlinear stretched surface with variable thickness. The heat transfer phenomenon is discussed through melting. The system of nonlinear ordinary differential equations is attained by considering proper transformations. Convergent series solutions of velocity and temperature are developed. Fluid flow, temperature, skin friction coefficient and Nusselt number are examined through graphs for different parameters. It is noted that velocity and temperature decrease with decreasing the wall thickness parameter. It is also revealed that the temperature distribution enhances for increasing values of the Prandtl number. Here the velocity field reduces for increasing values of the melting parameter.

1 Introduction

In industrial and engineering applications the fluid flow by a stretching sheet has obtained great importance. It has many applications in the manufacture of foods, liquid films in condensation process, rubber sheets, aerodynamic extraction of polymer and paper production etc. For these processes the level of the final product is based on the kinematics of the stretching and cooling rate. Experience of heat transfer in the stretched flow of a ferromagnetic liquid is described by Majeed *et al.* [1]. The impact of hydromagnetic and heat transfer in a micropolar fluid flow by a stretching surface is described by Mahmood *et al.* [2]. Rashidi *et al.* [3] interpreted the boundary layer nanofluid flow with effective Prandtl number. Hayat *et al.* [4] discussed the stretched flow of a non-Newtonian fluid with magnetohydrodynamic and nanoparticles effects. Khan *et al.* [5] discussed buoyancy and radiative impacts in the stretched nanofluid flow. Chandrasekar and Kasiviswanathan [6] analyzed the nanofluid flow with heat and mass transfer over a stretching sheet. Chen *et al.* [7] investigated the time-dependent Maxwell fluid flow bounded by a stretching sheet. Abbas *et al.* [8] examined slip flow by a stretching cylinder. Rashidi *et al.* [9] demonstrated radiative flow of nanofluid past a stretching channel. The stretched flow of water-based nanofluid in the presence of heat transfer is presented by Nadeem *et al.* [10].

Applications of non-Newtonian fluids in technology and industry (like oil recovery, polymer, food processing and nourishment preparing etc.) cannot be neglected. The constitutive relationship of the stress and rate of the strain is very complex in a non-Newtonian fluid. In the second-grade fluid only normal stress features are predicted. On the other hand, the third-grade fluid evaluates both the normal stresses and the shear thickening/thinning phenomena. Wang *et al.* [11] presented the impact of electromagnetohydrodynamic flow of the third-grade fluid between two parallel plates. Hayat *et al.* [12] demonstrated the behavior of heat transfer and magnetic field in a third-grade fluid flow over a stretching surface. Nadeem *et al.* [13] analyzed the mass transfer phenomenon in a third-grade fluid flow. Hussain *et al.* [14] illustrated the influences of viscous dissipation and hydromagnetics in the flow of a third-grade fluid. A third-grade fluid flow comprising magnetohydrodynamics in the stretched sheet is described by Rashidi *et al.* [15]. The mass transfer in a third-grade fluid along the vertical channel is discussed by Farooq *et al.* [16]. Abbasbandy and Hayat [17] focused on a time-dependent stretched flow of a third-grade fluid saturating the porous medium. Keimanesh *et al.* [18] investigated the third-grade fluid flow between two parallel plates.

Magnetohydrodynamic is a branch of fluid dynamics just to investigate the fluid motion in the presence of a magnetic field. MHD has many applications in flow meters, pumps, accelerators, MHD generators, blood pumping,

[a] e-mail: mi_qau@yahoo.com (corresponding author)

hyperthermia and cancer therapy inspection. Moreover the properties of magnetohydrodynamics are significant in cancer treatment, nuclear fuels treatment and blood pump machine. Gireesha *et al.* [19] studied the stagnation point flow of a nanofluid with magnetohydrodynamics. MHD viscoelastic flow with the Cattaneo-Christov heat flux model is illustrated by Li *et al.* [20]. MHD nanofluid flow with Hall effects over a permeable sheet is explored by Makinde *et al.* [21]. Sheikh and Abbas [22] investigated the MHD flow of a viscoelastic fluid and heat transfer through heat generation/absorption. The MHD non-Newtonian fluid flow over a stretching surface is illustrated by Rashidi *et al.* [15]. The MHD radiative flow of Jeffery fluid by an exponentially stretching sheet is inspected by Hayat *et al.* [23]. Some of the investigations related to the MHD can be seen in refs. [24–30].

The phenomenon of melting heat transfer has promising applications in engineering processes. In the developed technological processes melting plays a prominent role. Melting heat transfer is useful in thawing of frozen ground, casting of manufacturing process, heat transportation melting of permafrost, magma solidification, cyrstal growth, optimal utilization of energy and preparation of semiconductors material. Epstein and Cho [31] discussed melting heat transfer in a flow by a flat plate. Ahmad and Pop [32] presented the boundary layer flow of a viscous fluid with porous medium and melting phenomenon. Awais *et al.* [33] discussed the melting heat transfer in the flow of a Burgers fluid. The Williamson nanofluid flow over a non-linear stretching sheet with melting heat transfer is demonstrated by Hayat *et al.* [34]. The fluid flow in a porous medium through melting process has been discussed by Kameswaran *et al.* [35]. Krishnamurthy *et al.* [36] presented effects of melting and radiation in flow by a stretching sheet. Wang *et al.* [37] examined the process of solidification and melting along a vertical shell with thermophysical properties. Heat transfer analysis through melting and Joule heating in a nanofluid flow has been discussed by Hayat *et al.* [38].

In this paper we study the behavior of the MHD flow of a third-grade fluid over a variable-thickness moving surface. The stretching velocity is considered nonlinear. We also considered the heat transfer phenomenon through the melting process. To attain the convergent series solution we use the homotopy analysis method [39–44]. The various parameters involved in velocity and temperature are explored through plots. The skin friction coefficient and surface heat transfer rate are also examined.

2 Formulation

We explored the two-dimensional flow of the third-grade fluid over a non-linear stretching sheet with variable thickness. Heat transfer is examined through the melting process. The thickness of the sheet is $y = B(x+b)^{\frac{1-n}{2}}$. We take T_m, the melting temperature, and T_∞, the ambient temperature, such that $T_\infty > T_m$.

The basic equations are

$$\operatorname{div}\mathbf{V} = 0, \tag{1}$$

$$\rho\frac{\mathrm{d}\mathbf{V}}{\mathrm{d}t} = \operatorname{div}\mathbf{T} + \mathbf{J}\times\mathbf{B}, \tag{2}$$

$$\rho c_p\frac{\partial T}{\partial t} + (\mathbf{V}\cdot\nabla)T = -\operatorname{div}\mathbf{q}, \tag{3}$$

in which $\mathbf{V}$ denotes the velocity field, ρ the density of fluid, $\mathbf{J}$ the current density, $\mathbf{T}$ the Cauchy stress tensor, $\mathbf{B}$ the total magnetic field, c_p the specific heat and T the temperature of the fluid.

The constitutive relation of the stress tensor for a third-grade fluid is

$$\mathbf{T} = -p\mathbf{I} + \mu\mathbf{A}_1 + \alpha_1\mathbf{A}_2 + \alpha_2\mathbf{A}_1^2 + \beta_3(\operatorname{tr}\mathbf{A}_1^2)\mathbf{A}_1, \tag{4}$$

where

$$\mathbf{A}_1 = \operatorname{grad}\mathbf{V} + (\operatorname{grad}\mathbf{V})^T, \tag{5}$$

$$\mathbf{A}_2 = \frac{\mathrm{d}\mathbf{A}_1}{\mathrm{d}t} + \mathbf{A}_1\mathbf{L} + \mathbf{L}^T\mathbf{A}_1, \quad L = \operatorname{grad}\mathbf{V}. \tag{6}$$

Also the heat flux is

$$\mathbf{q} = -k\operatorname{grad}T, \tag{7}$$

where μ denotes the dynamic viscosity, $\mathbf{I}$ the identity tensor, α_1, α_2, β_3 the material constants and k the thermal conductivity.

Velocity field is defined by

$$\mathbf{V} = [u(x,y), \mathrm{v}(x,y), 0], \tag{8}$$

in which $u(x,y)$ and $\mathrm{v}(x,y)$ are components of velocity field $\mathbf{V}$.

The boundary layer equations are

$$\frac{\partial u}{\partial x}+\frac{\partial \mathrm{v}}{\partial y}=0, \tag{9}$$

$$u\frac{\partial u}{\partial x}+\mathrm{v}\frac{\partial u}{\partial y}=\nu\frac{\partial^2 u}{\partial y^2}+\frac{\alpha_1}{\rho}\left(u\frac{\partial^3 u}{\partial x\partial y^2}+\frac{\partial u}{\partial x}\frac{\partial^2 u}{\partial y^2}+3\frac{\partial u}{\partial y}\frac{\partial^2 u}{\partial x\partial y}+\mathrm{v}\frac{\partial^3 u}{\partial y^3}\right)+\frac{2\alpha_2}{\rho}\frac{\partial u}{\partial y}\frac{\partial^2 u}{\partial x\partial y}+\frac{6\beta_3}{\rho}\left(\left(\frac{\partial u}{\partial y}\right)^2\frac{\partial^2 u}{\partial y^2}\right)-\frac{\sigma B_0^2 u}{\rho}, \tag{10}$$

$$\rho C_p\left(u\frac{\partial T}{\partial x}+\mathrm{v}\frac{\partial T}{\partial y}\right)=k\frac{\partial^2 T}{\partial y^2}. \tag{11}$$

The corresponding boundary conditions are

$$u=u(x,y)=U_0(x+b)^m,\quad \mathrm{v}=0,\quad T=T_m\quad \text{at } y=B(x+b)^{\frac{1-n}{2}}, \tag{12}$$

$$u\to 0,\quad \mathrm{v}\to 0,\quad T\to T_\infty\quad \text{as } y\to\infty \tag{13}$$

and

$$k\left(\frac{\partial T}{\partial y}\right)_{y=B(x+b)^{\frac{1-n}{2}}}=\rho\left[\lambda+C_s(T_m-T_0)\right]\mathrm{v}\left(x,y=B(x+b)^{\frac{1-n}{2}}\right). \tag{14}$$

Here ν denotes the kinematic viscosity of the fluid, σ the electrical conductivity and B_0 the strength of the magnetic field. The shape parameter n is used to control the type of the motion, the behavior of the boundary layer and the shape of the surface. We have three cases for wall thickness parameter n. For $n=1$ the surface is flat. For $n<1$ the wall thickness parameter increases whereas the wall thickness parameter decreases for $n>1$. As this parameter controls the type of motion so $n=0$ represents the linear motion, $n<1$ the deceleration motion and $n>1$ accelerated motion.

Transformations are considered as

$$\eta=\sqrt{\frac{(m+1)U_0(x+b)^{n-1}}{2\nu}}y,\qquad \psi=\sqrt{\frac{2}{n+1}\nu U_0(x+b)^{n+1}}F(\eta),\qquad \Theta(\eta)=\frac{T-T_m}{T_\infty-T_m},$$

$$u=U_0(x+b)^m F'(\eta),\qquad \mathrm{v}=-\sqrt{\frac{(n+1)\nu U_0(x+b)^{n-1}}{2}}\left[F(\eta)+\eta F'(\eta)\frac{n-1}{n+1}\right], \tag{15}$$

in which F denotes the dimensionless stream function and Θ the dimensionless temperature. The continuity equation (9) is automatically satisfied and eqs. (10)–(14) take the form

$$F'''+FF''-\frac{2n}{n+1}F'^2+\epsilon_1\left[(3n-1)F'F'''+2(n-1)\eta F''F'''+\frac{3(3n-1)}{2}F''^2-\frac{n+1}{2}FF''''\right]$$
$$+\epsilon_2\left[(3n-1)F''^2+(n-1)\eta F''F'''\right]+6\phi\,\mathrm{Re}_x^{1/2}\frac{n+1}{2}F''^2F'''-\frac{2A}{n+1}F'=0, \tag{16}$$

$$\frac{1}{\mathrm{Pr}}\Theta''+F\Theta'=0, \tag{17}$$

$$F'(\alpha)=1,\quad M\Theta'(\alpha)+\mathrm{Pr}\left[F(\alpha)+\frac{n-1}{n+1}\alpha\right],\quad \Theta(\alpha)=0, \tag{18}$$

$$F'(\infty)\to 0,\qquad \Theta(\infty)\to 1. \tag{19}$$

Here $\alpha=B\sqrt{\frac{(n+1)U_0}{2\nu}}$ is the wall thickness parameter.

Writing

$$f(\xi)=f(\eta-\alpha)=F(\eta), \tag{20}$$

and using eq. (20), eqs. (16)–(19) become

$$f'''+ff''-\frac{2n}{n+1}f'^2+\epsilon_1\left[(3n-1)f'f'''+2(n-1)\eta f''f'''+\frac{3(3n-1)}{2}f''^2-\frac{n+1}{2}ff''''\right]$$
$$+\epsilon_2\left[(3n-1)f''^2+(n-1)\eta f''f'''\right]+6\phi\,\mathrm{Re}_x^{1/2}\frac{n+1}{2}f''^2f'''-\frac{2A}{n+1}f'=0, \tag{21}$$

$$\frac{1}{\mathrm{Pr}}\theta''+f\theta'=0, \tag{22}$$

where the boundary conditions are

$$f'(0)=1, \quad M\theta'(0)+\Pr\left[f(0)+\frac{n-1}{n+1}\alpha\right], \quad \theta(0)=0,$$
$$f'(\infty)\to 0, \qquad \theta(\infty)\to 1, \tag{23}$$

in which $\epsilon_1=\frac{\alpha_1 U_0}{\mu}(x+b)^{n-1}$, $\epsilon_2=\frac{\alpha_2 U_0}{\mu}(x+b)^{n-1}$ and $\phi=\frac{\beta_3 U_0}{\mu}(x+b)^{n-1}$ are the material parameters of a third-grade fluid, $\mathrm{Re}_x^{1/2}=\sqrt{\frac{U_0(x+b)^{n-1}}{\nu}}$ the local Reynolds number, $A=\frac{\sigma B_0^2}{\rho U_0(x+b)^{n-1}}$ the Hartman number, $\Pr=\frac{\mu C_p}{k}$ the Prandtl number and $M=\frac{C_p(T_\infty-T_m)}{\lambda+C_s(T_m-T_0)}$ the melting parameter.

The mathematical formulation of the skin friction coefficient C_f and of the local Nusselt number Nu_x can be written as

$$C_f=\frac{\tau_w}{\rho U_w^2}, \qquad Nu_x=\frac{(x+b)q_w}{k(T_\infty-T_m)}, \tag{24}$$

where

$$\tau_w=\left[\mu\frac{\partial u}{\partial y}+\alpha_1\left(u\frac{\partial^2 u}{\partial x\partial y}+2\frac{\partial u}{\partial x}\frac{\partial u}{\partial y}+\mathrm{v}\frac{\partial^2 u}{\partial y^2}\right)+2\beta_3\left(\frac{\partial u}{\partial y}\right)^3\right]_{y=B(x+b)^{\frac{1-n}{2}}}, \tag{25}$$

$$q_w=-k\left(\frac{\partial T}{\partial y}\right)_{y=B(x+b)^{\frac{1-n}{2}}}. \tag{26}$$

The non-dimensionalised quantities of the skin friction coefficient C_f and of the local Nusselt number Nu_x become

$$\mathrm{Re}_x^{1/2}C_f=\left[f''(0)+\epsilon_1\left(\frac{7n-1}{2}f'(0)f''(0)+\alpha(n-1)f''^2(0)-\frac{n+1}{2}f(0)f'''(0)\right)+2\phi\,\mathrm{Re}_x^{1/2}\,\frac{n+1}{2}f''^3(0)\right]\sqrt{\frac{n+1}{2}}, \tag{27}$$

$$\mathrm{Re}_x^{-1/2}Nu_x=-\theta'(0)\sqrt{\frac{n+1}{2}}. \tag{28}$$

3 Homotopic solutions

Here we utilized the homotopy technique for the solution of non-linear differential equation. The homotopy technique is used to obtain a convergent series solution for the non-linear system. We take the initial guesses for unknown function and auxiliary operators in the form

$$f_0(\xi)=\alpha\frac{1-n}{n+1}+(1-e^{-\xi})-\frac{M}{\Pr}, \qquad \theta_0(\xi)=1-e^{-\xi}, \tag{29}$$
$$\mathcal{L}_f=f'''-f', \qquad \mathcal{L}_\theta=\theta''-\theta, \tag{30}$$
$$\mathcal{L}_f(c_1+c_2e^{\xi}+c_3e^{-\xi})=0, \qquad \mathcal{L}_\theta(c_4e^{\xi}+c_5e^{-\xi})=0, \tag{31}$$

in which c_1-c_5 represent the constants.

The zeroth-order deformation problems are

$$(1-p)\mathcal{L}_f\left[\hat{f}(\xi,p)-f_0(\xi)\right]=p\hbar_f\mathcal{N}_f[\hat{f}(\xi,p)], \tag{32}$$
$$(1-p)\mathcal{L}_\theta\left[\hat{\theta}(\xi,p)-\theta_0(\xi)\right]=p\hbar_\theta\mathcal{N}_\theta[\hat{\theta}(\xi,p),\hat{f}(\xi,p)], \tag{33}$$

where p is the embedding parameter varying from 0 to 1, $\hbar_f$ and $\hbar_\theta$ denote the auxiliary parameters and $\mathcal{N}_f$ and $\mathcal{N}_\theta$ are

$$\begin{aligned}\mathcal{N}_f\left[\hat{f}(\xi,p)\right] &= \frac{\partial^3\hat{f}(\xi,p)}{\partial\xi^3} + \hat{f}(\xi,p)\frac{\partial^2\hat{f}(\xi,p)}{\partial\xi^2} - \frac{2n}{n+1}\left(\frac{\partial\hat{f}(\xi,p)}{\partial\xi}\right)^2 \\ &+ \epsilon_1\Bigg((3n-1)\frac{\partial\hat{f}(\xi,p)}{\partial\xi}\frac{\partial^3\hat{f}(\xi,p)}{\partial\xi^3} + 2(n-1)\xi \\ &\frac{\partial^2\hat{f}(\xi,p)}{\partial\xi^2}\frac{\partial^3\hat{f}(\xi,p)}{\partial\xi^3} + \frac{3(3n-1)}{2}\left(\frac{\partial^2\hat{f}(\xi,p)}{\partial\xi^2}\right)^2 - \frac{n+1}{2}\hat{f}(\xi,p)\frac{\partial^4\hat{f}(\xi,p)}{\partial\xi^4}\Bigg) \\ &+ \epsilon_2\left((3n-1)\left(\frac{\partial^2\hat{f}(\xi,p)}{\partial\xi^2}\right)^2 + (n-1)\xi\frac{\partial^2\hat{f}(\xi,p)}{\partial\xi^2}\frac{\partial^3\hat{f}(\xi,p)}{\partial\xi^3}\right) + 6\phi\,\mathrm{Re}_x^{1/2}\,\frac{n+1}{2}\left(\frac{\partial^2\hat{f}(\xi,p)}{\partial\xi^2}\right)^2 \\ &\frac{\partial^3\hat{f}(\xi,p)}{\partial\xi^3} - \frac{2A}{n+1}\frac{\partial\hat{f}(\xi,p)}{\partial\xi}, \end{aligned} \tag{34}$$

$$\mathcal{N}_\theta\left[\hat{\theta}(\xi,p),\hat{f}(\xi,p)\right] = \frac{1}{\mathrm{Pr}}\frac{\partial^2\hat{\theta}(\xi,p)}{\partial\xi^2} + \hat{f}(\xi,p)\frac{\partial\hat{\theta}(\xi,p)}{\partial\xi}, \tag{35}$$

with boundary conditions

$$\begin{aligned}&\hat{f}'(0,p) = 1, M\hat{\theta}'(0,p) + \mathrm{Pr}\left[\hat{f}(0,p) + \frac{n-1}{n+1}\alpha\right] = 0, \qquad \hat{f}'(\infty,p) = 0, \\ &\hat{\theta}(0,p) = 0, \qquad \hat{\theta}(\infty,p) = 1. \end{aligned} \tag{36}$$

The m-th–order equations are

$$\mathcal{L}_f\left[f_m(\xi) - \chi_m f_{m-1}(\xi)\right] = \hbar_f\mathcal{R}_{f,m}(\xi), \tag{37}$$

$$\mathcal{L}_\theta\left[\theta_m(\xi) - \chi_m\theta_{m-1}(\xi)\right] = \hbar_\theta\mathcal{R}_{\theta,m}(\xi), \tag{38}$$

$$\chi_m = \begin{cases} 0, & m \le 1, \\ 1, & m > 1, \end{cases} \tag{39}$$

$$\begin{aligned}\mathcal{R}_{f,m}(\xi) &= f'''_{m-1} + \sum_{k=0}^{m-1}\left[f_{m-1-k}f''_k - \frac{2n}{n+1}f'_{m-1-k}f'_k\right] \\ &+ \epsilon_1\sum_{k=0}^{m-1}\left[(3n-1)f'_{m-1-k}f'''_k + 2(n-1)\xi f''_{m-1-k}f'''_k + \frac{3(3n-1)}{2}f''_{m-1-k}f''_k - \frac{n+1}{2}f_{m-1-k}f^{iv}_k\right] \\ &+ \epsilon_2\sum_{k=0}^{m-1}\left[(3n-1)f''_{m-1-k}f''_k + (n-1)\xi f''_{m-1-k}f'''_k\right] - \frac{2A}{n+1}f'_{m-1} \\ &+ \sum_{l=0}^{m-1}f''_{m-1-l}\left(6\phi\,\mathrm{Re}_x^{1/2}\,\frac{n+1}{2}\sum_{j=0}^{l}f''_{l-j}f'''_j\right), \end{aligned} \tag{40}$$

$$\mathcal{R}_{\theta,m}(\xi) = \frac{1}{\mathrm{Pr}}\theta''_{m-1} + \sum_{l=0}^{m-1}\left[\theta'_{m-1-l}f_l\right], \tag{41}$$

with boundary conditions

$$f'_m(0) = M\theta'_m(0) + \mathrm{Pr}\,f_m(0) = f'_m(\infty) = \theta_m(0) = \theta_m(\infty) = 0. \tag{42}$$

The general solutions (f_m,θ_m) including the special solutions (f^*_m,θ^*_m) are defined by

$$\begin{aligned}f_m(\xi) &= f^*_m(\xi) + c_1 + c_2e^{\xi} + c_3e^{-\xi}, \\ \theta_m(\xi) &= \theta^*_m(\xi) + c_4e^{\xi} + c_5e^{-\xi}. \end{aligned} \tag{43}$$

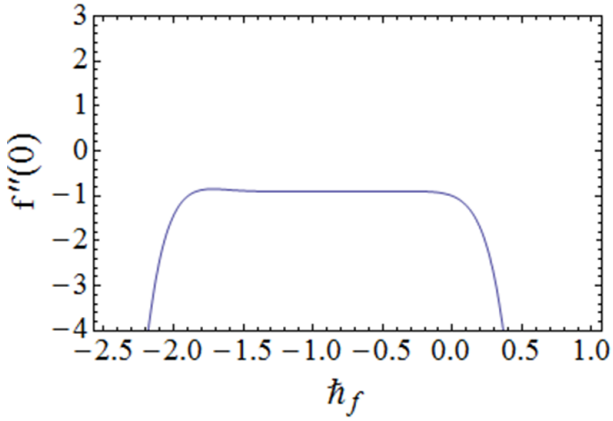

Fig. 1. $\hbar$-curve for $f''(0)$ when $M = 0.5$, $\Pr = 1.9$, $A = 0.7$, $\alpha = 0.1$, $\epsilon_1 = \epsilon_2 = \phi = \mathrm{Re}_x^{1/2} = 0.1$ and $n = 1.5$.

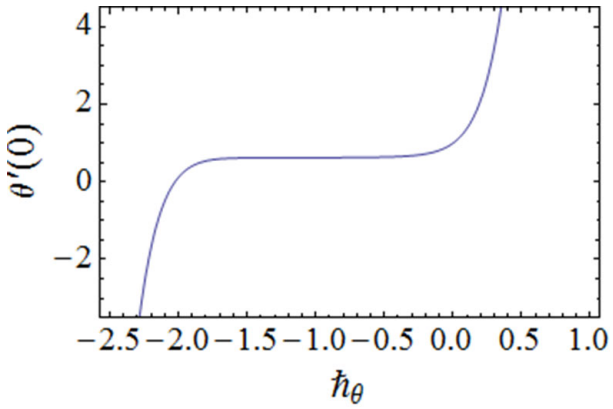

Fig. 2. $\hbar$-curve for $\theta'(0)$ when $M = 0.5$, $\Pr = 1.9$, $A = 0.7$, $\alpha = 0.1$, $\epsilon_1 = \epsilon_2 = \phi = \mathrm{Re}_x^{1/2} = 0.1$ and $n = 1.5$.

Table 1. Convergence of HAM solutions for various orders of approximations when $M = 0.5$, $\Pr = 1.9$, $A = 0.7$, $\alpha = 0.1$, $\epsilon_1 = \epsilon_2 = \phi = \mathrm{Re}_x^{1/2} = 0.1$ and $n = 1.5$.

Order of approximations	$-f''(0)$	$\theta'(0)$
1	0.9162	0.6237
3	0.9001	0.6267
5	0.8990	0.6231
7	0.8984	0.6206
8	0.8983	0.6203
9	0.8983	0.6198
20	0.8983	0.6198
30	0.8983	0.6198
40	0.8983	0.6198
45	0.8983	0.6198

4 Convergence analysis

Homotopic procedure is adopted to obtain the convergent series solutions. The region of convergence is parallel to $\hbar$-axis (see figs. 1 and 2). It is observed that the suitable range of parameter $\hbar_f$ is $[-1.5, -0.6]$ and $\hbar_\theta$ is $[-1.5, -0.8]$. The convergent series solution is obtained for $\hbar_f = -0.6$ and $\hbar_\theta = -1.3$.

Table 1 illustrates the convergence of series solutions for basic equations. Here for the convergence of the velocity the 8th order of approximation is enough, whereas the 9th order of approximation is sufficient for the temperature.

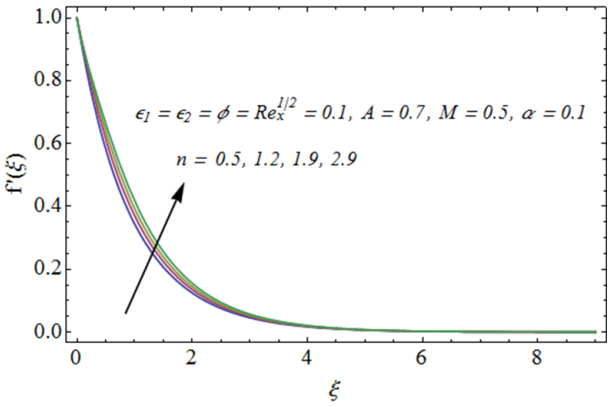

Fig. 3. Impact of n on velocity.

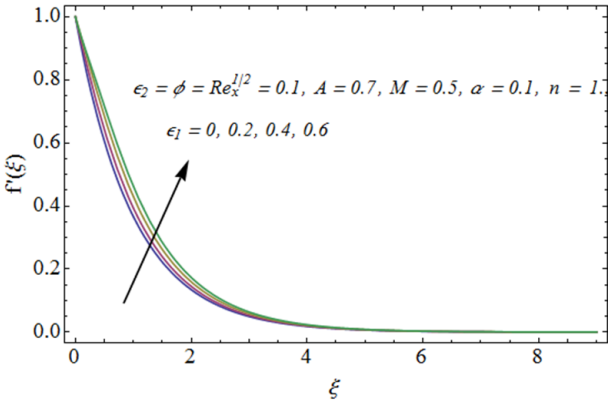

Fig. 4. Impact of ϵ_1 on velocity.

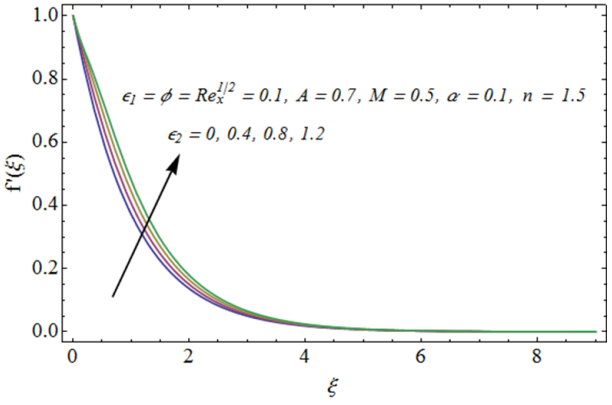

Fig. 5. Impact of ϵ_2 on velocity.

5 Discussion

5.1 Dimensionless velocity profiles

Figure 3 illustrates the increasing behavior of n *vs.* velocity $f'(\xi)$. It is found that the thickness of the wall decreases for larger values of n which increases the fluid velocity. Figures 4, 5 illustrate the variation of material parameters ϵ_1 and ϵ_2. It is seen that the velocity increases for increasing values of ϵ_1 and ϵ_2. The boundary layer thickness enhances for increasing values of fluid parameters. The velocity increases. Figure 6 describes the variation of Hartman number A on the velocity profile. Larger values of the Hartman number reduces the velocity. The influence of the melting parameter M on velocity $f'(\xi)$ is illustrated in fig. 7. Here the velocity decreases for increasing values of M. Figures 8 and 9 shows the decreasing behavior of ϕ and $\mathrm{Re}_x^{1/2}$ *vs.* velocity profile.

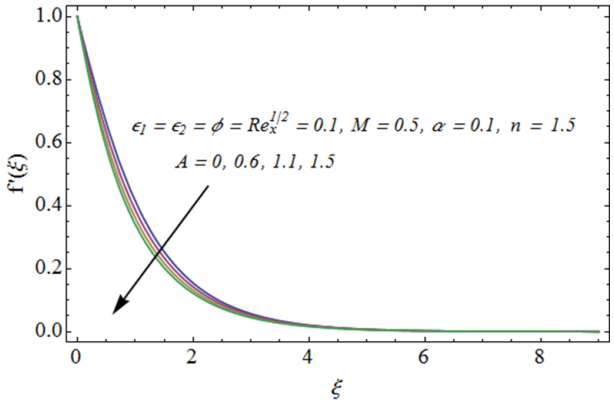

Fig. 6. Impact of A on velocity.

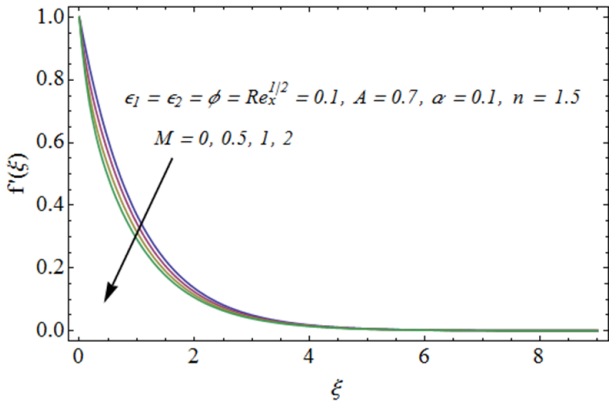

Fig. 7. Impact of M on velocity.

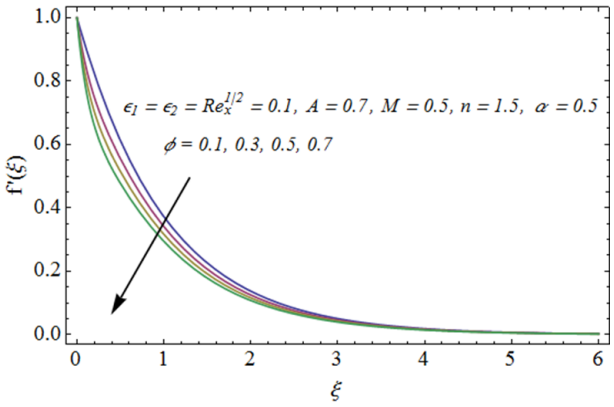

Fig. 8. Impact of ϕ on velocity.

5.2 Dimensionless temperature profiles

Figure 10 exhibits the variation of melting parameter with $\theta(\xi)$. It is clear that large values of the melting parameter correspond to lower temperature. Figure 11 analyzes the impact of Prandtl number on the temperature profile $\theta(\xi)$. Here the temperature increases when Pr is enhanced. Temperature is a decreasing function of the wall thickness parameter α (see fig. 12).

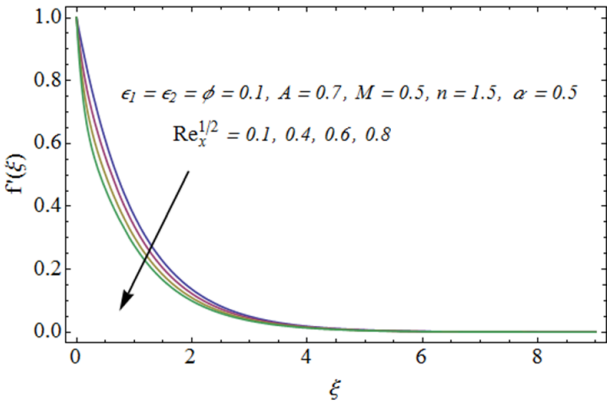

Fig. 9. Impact of ϕ_1 on velocity.

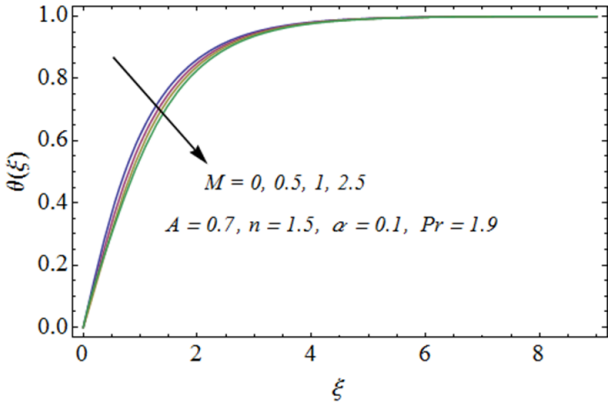

Fig. 10. Impact of M on $\theta(\xi)$.

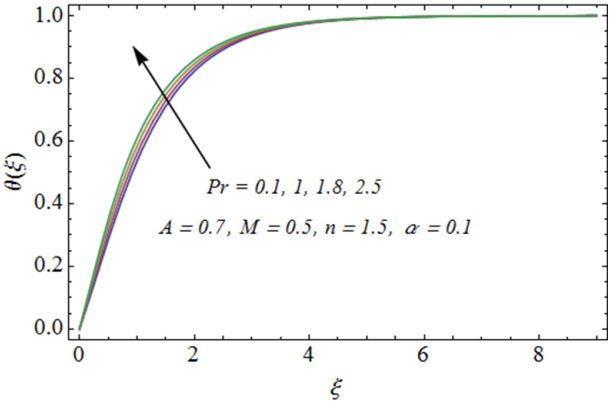

Fig. 11. Impact of Pr on $\theta(\xi)$.

5.3 Skin friction coefficient

The impact of embedded variables on the skin friction coefficient $\mathrm{Re}_x^{1/2} C_f$ is characterized in figs. 13-14. Figure 13 illustrates the reduction of the skin friction coefficient via ϵ_1 and higher values of the shape parameter n. From fig. 14 it is seen that the skin friction coefficient decreases for increasing values of ϵ_1. Figure 15 shows that for larger values of ϵ_2 the skin friction coefficient $\mathrm{Re}_x^{1/2} C_f$ decreases.

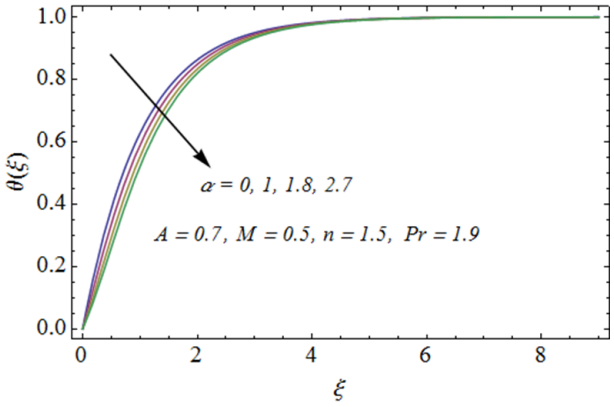

Fig. 12. Impact of α on $\theta(\xi)$.

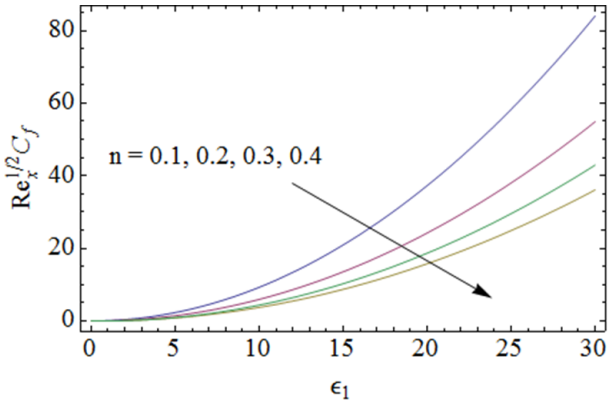

Fig. 13. Impact of n on $\mathrm{Re}_x^{1/2}\, C_f$.

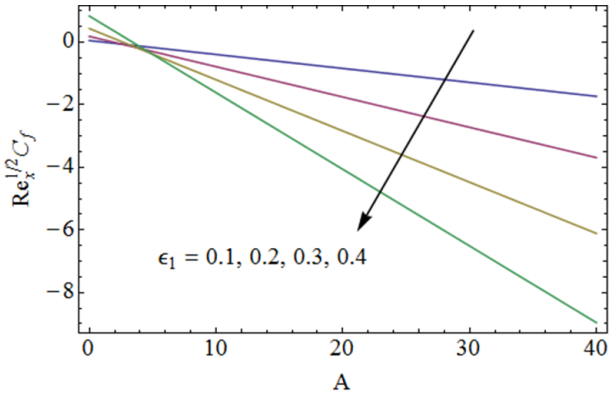

Fig. 14. Impact of ϵ_1 on $\mathrm{Re}_x^{1/2}\, C_f$.

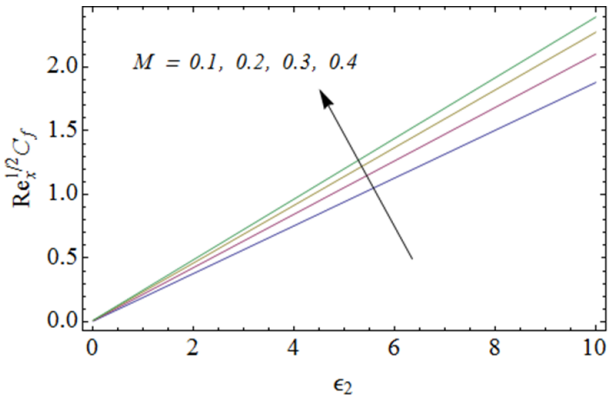

Fig. 15. Impact of ϵ_2 on $\mathrm{Re}_x^{1/2}\, C_f$.

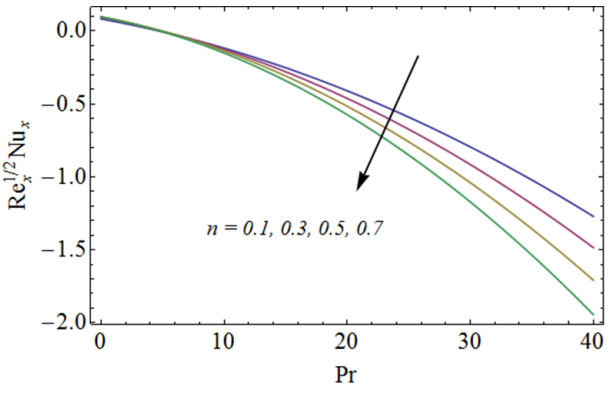

Fig. 16. Impact of n on $\mathrm{Re}_x^{-1/2}\, Nu_x$.

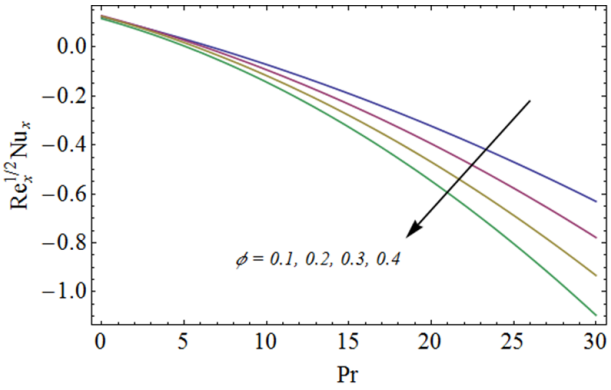

Fig. 17. Impact of ϕ on $\mathrm{Re}_x^{-1/2}\, Nu_x$.

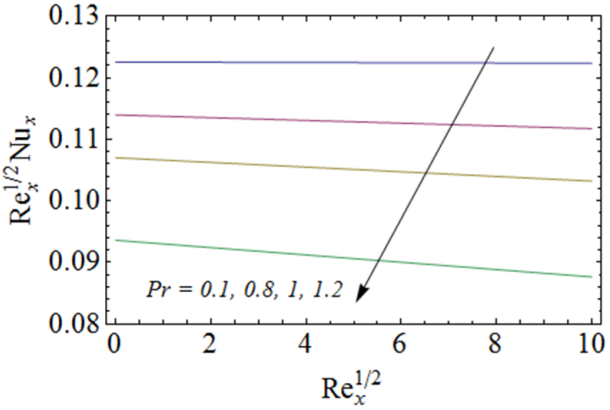

Fig. 18. Impact of Pr on $\mathrm{Re}_x^{-1/2}\, Nu_x$.

5.4 Nusselt number

Figure 16 depicts the decreasing behavior of n on the surface heat transfer rate $\mathrm{Re}_x^{-1/2}\, Nu_x$ via Pr. The impact of ϕ on the Nusselt number $\mathrm{Re}_x^{-1/2}\, Nu_x$ via Pr is displayed in fig. 17. Here we noticed that surface heat transfer rate $\mathrm{Re}_x^{-1/2}\, Nu_x$ reduces for higher values of ϕ via Pr. Figure 18 depicts the decreasing behavior of Pr on the surface heat transfer rate $\mathrm{Re}_x^{-1/2}\, Nu_x$.

6 Main results

The stretched flow of a third-grade fluid with variable thickness and melting heat transfer is explored here. The main observation of the given problem are summarized as follows:

- The velocity profile is a decreasing function of the melting parameter and the wall thickness parameter.
- The velocity is dominant for the shape parameter.
- Increasing values of the Hartman number reduce the velocity profile.
- Reduction in temperature distribution is observed for higher values of the melting parameter.
- Increasing values of Pr yield on an increase in the temperature.

References

1. A. Majeed, A. Zeeshan, R. Ellahi, J. Mol. Liq. **223**, 528 (2016).
2. A. Mahmood, B. Chen, A. Ghaffari, J. Magn. & Magn. Mater. **416**, 329 (2016).
3. M.M. Rashidi, N.V. Ganesh, A.K.A. Hakeem, B. Ganga, G. Lorenzini, Int. J. Heat Mass Transfer **98**, 616 (2016).
4. T. Hayat, A. Aziz, T. Muhammad, B. Ahmad, J. Magn. & Magn. Mater. **408**, 99 (2016).
5. J.A. Khan, M. Mustafa, T. Hayat, A. Alsaedi, Int. J. Heat Mass Transfer **86**, 158 (2015).
6. M. Chandrasekar, M.S. Kasiviswanathan, Proc. Eng. **127**, 493 (2015).
7. S. Chen, L. Zheng, B. Shen, X. Chen, Theor. Appl. Mech. Lett. **5**, 262 (2015).
8. Z. Abbas, S. Rasool, M.M. Rashidi, Ain Shams Eng. J. **6**, 939 (2015).
9. M.M. Rashidi, N.V. Ganesh, A.K.A. Hakeem, B. Ganga, J. Mol. Liq. **198**, 234 (2014).
10. S. Nadeem, R.U. Haq, Z.H. Khan, Alex. Eng. J. **53**, 219 (2014).
11. L. Wang, Y. Jian, Q. Liu, F. Li, L. Chang, Phys. Eng. Asp. **494**, 87 (2016).
12. T. Hayat, M.I. Khan, M. Waqas, A. Alsaedi, T. Yasmeen, Chin. J. Chem. Eng. (2016) DOI: 10.1016/j.cjche.2016.06.008.
13. S. Nadeem, S. Saleem, Int. J. Heat Mass Transfer **85**, 1041 (2015).
14. T. Hussain, S.A. Shehzad, T. Hayat, A. Alsaedi, AIP Adv. **5**, 087169 (2015).
15. M.M. Rashidi, S. Bagheri, E. Momoniatd, N. Freidoonimehre, Ain Shams Eng. J. **8**, 77 (2017).
16. U. Farooq, T. Hayat, A. Alsaedi, S. Liao, Appl. Math. Comput. **242**, 528 (2014).
17. S. Abbasbandy, T. Hayat, Commun. Nonlinear Sci. Numer. Simul. **16**, 3140 (2011).
18. M. Keimanesh, M.M. Rashidi, A.J. Chamkha, R. Jafari, Comp. Math. App. **62**, 2871 (2011).
19. B.J. Gireesha, B. Mahanthesh, I.S. Shivakumara, K.M. Eshwarappa, Eng. Sci. Tech. Int. J. **19**, 313 (2016).
20. J. Li, L. Zheng, L. Liu, J. Mol. Liq. **221**, 19 (2016).
21. O.D. Makinde, T. Iskander, F. Mabood, W.A. Khan, M.S. Tshehla, J. Mol. Liq. **221**, 778 (2016).
22. M. Sheikh, Z. Abbas, J. Magn. & Magn. Mater. **396**, 204 (2015).
23. T. Hayat, S. Asad, M. Mustafa, A. Alsaedi, Comput. Fluids **108**, 179 (2015).
24. N.S. Akbar, M. Raza, R. Ellahi, Eur. Phy. J. Plus **129**, 155 (2014).
25. M.M. Bhatti, A. Zeeshan, R. Ellahi, N. Ijaz, J. Mol. Liq. **230**, 237 (2017).
26. M.M. Bhatti, A. Zeeshan, R. Ellahi, Microvasc. Res. **110**, 32 (2017).
27. R. Ellahi, M.H. Tariq, M. Hassan, K. Vafai, J. Mol. Liq. **229**, 339 (2017).
28. R. Ellahi, M.M. Bhatti, I. Pop, Int. J. Numer. Methods Heat Fluid Flow **26**, 1802 (2016).
29. A.A. Khan, S. Muhammad, R. Ellahi, Q.M.Z. Zia, J. Magn. **21**, 273 (2016).
30. R. Ellahi, F. Hussain, J. Magn. & Magn. Mater. **393**, 284 (2015).
31. M. Epstein, D.H. Cho, J. Heat Transf. **98**, 531 (1976).
32. S. Ahmad, I. Pop, Transp. Porous Media **102**, 317 (2014).
33. M. Awais, T. Hayat, A. Alsaedi, J. Egypt. Math. Soc. **23**, 410 (2015).
34. T. Hayat, G. Bashir, M. Waqas, A. Alsaedi, J. Mol. Liq. **223**, 836 (2016).
35. P.K. Kameswaran, K. Hemalatha, M.V.D.N.S. Madhavi, Adv. Powder Tech. **27**, 417 (2016).
36. M.R. Krishnamurthy, B.C. Prasannakumara, B.J. Gireesha, R.S.R. Gorla, Eng. Sci. Tech. Int. J. **19**, 53 (2016).
37. Y. Wang, L. Wang, N. Xie, X. Lin, H. Chen, Int. J. Heat Mass Transfer **99**, 770 (2016).
38. T. Hayat, M. Imtiaz, A Alsaedi, Adv. Pow. Tech. **27**, 1301 (2016).
39. S. Abbasbandy, M. Yurusoy, H. Gulluce, Math. Comput. Appl. **19**, 124 (2014).
40. U. Farooq, Y.L. Zhao, T. Hayat, A. Alsaedi, S.J. Liao, Comput. Fluids **111**, 69 (2015).
41. T. Hayat, M. Imtiaz, A. Alsaedi, R. Mansoor, J. Aerospace Eng. (2015) DOI: 10.1061/(ASCE)AS.1943-5525.0000533.
42. D.D. Ganji, M. Abbasi, J. Rahimi, M. Gholami, I. Rahimipetroudi, Front. Mech. Eng. **9**, 270 (2014).
43. T. Hayat, M. Imtiaz, A. Alsaedi, J. Magn. & Magn. Mater. **395**, 294 (2015).
44. T. Hayat, S. Qayyum, M. Imtiaz, A. Alsaedi, PLoS ONE **11**, e0148662 (2016).